Journal of Materials Chemistry A

ROYAL SOCIETY OF CHEMISTRY

PAPER

View Article Online
View Journal

Cite this: DOI: 10.1039/d3ta00076a

Synthesis of high-purity Li_2S nanocrystals *via* metathesis for solid-state electrolyte applications†

William H. Smith, Saeed Ahmadi Vaselabadi and Colin A. Wolden *

Li_2S is the key precursor for synthesizing thio-LISICON electrolytes employed in solid state batteries. However, conventional synthesis techniques such as carbothermal reduction of Li_2SO_4 aren't suitable for the generation of low-cost, high-purity Li_2S. Metathesis, in which LiCl is reacted with Na_2S in ethanol, is a scalable synthesis method conducted at ambient conditions. The NaCl byproduct is separated from the resulting Li_2S solution, and the solvent is removed by evaporation and thermal annealing. However, the annealing process reveals the presence of oxygenated impurities in metathesis Li_2S that are not usually observed when recovering Li_2S from ethanol. In this work we investigate the underlying mechanism of impurity formation, finding that they likely derive from the decomposition of alkoxide species that originate from the alcoholysis of the Na_2S reagent. With this mechanism in mind, several strategies to improve Li_2S purity are explored. In particular, drying the metathesis Li_2S under H_2S at low temperature was most effective, resulting in high-purity Li_2S while retaining a beneficial nanocrystal morphology (~10 nm). Argyrodite electrolytes synthesized from this material exhibited essentially identical phase purity, ionic conductivity (3.1 mS cm^{-1}), activation energy (0.19 eV), and electronic conductivity (6.4×10^{-6} mS cm^{-1}) as that synthesized from commercially available battery-grade Li_2S.

Received 4th January 2023
Accepted 16th March 2023

DOI: 10.1039/d3ta00076a

rsc.li/materials-a

Introduction

Demand for energy storage is increasing rapidly as electricity generation shifts to intermittent sources of renewable electricity such as wind and solar along with increased electrification of transportation and industrial sectors. The lithium-ion battery (LIB) is the leading electrochemical energy storage technology due to its good performance (high energy density, good power capability, efficiency, and long lifetime) and relatively low energy cost (~100 USD per kW per h at the cell level).[1–3] However, conventional LIBs face several limitations: the intercalation materials used in LIBs are nearing their physicochemical limit in terms of energy density, which constrains electric vehicle range and limits the storage capacity of stationary installations.[4] Furthermore, LIBs suffer from poor performance at both high and low temperatures. The risk of thermal runaway leading to ignition of the flammable electrolyte reduces the maximum operating temperature of battery packs, and the poor ionic conductivity of the electrolyte at low temperatures limits performance of LIBs in cold weather.[5] Due to these limitations, complex thermal management systems are used to maintain ideal operating temperatures, leading to increases in system cost, mass, and volume.

Replacing the organic liquid electrolyte with alternatives, such as an inorganic solid-state electrolyte (SSE), has been suggested as an elegant solution to these myriad challenges. Solid-state electrolytes have been shown to possess improved compatibility with next-generation high-energy active materials based on alloying and conversion mechanisms, such as Si/Li-metal anodes and sulfur cathodes.[6–8] Solid-state electrolytes also exhibit superior thermal stability with greatly reduced risk of thermal runaway and satisfactory low-temperature performance.[9] Therefore, advanced batteries employing SSEs may achieve higher energy density with reduced need for complex thermal management systems. In addition to these benefits, all-solid-state batteries can be manufactured in a bipolar stack, where several cell layers are stacked in one package to yield the required operating voltage, rather than combining several individually packaged cells in series as is done with liquid-based cells.[10]

Sulfide SSEs are leading candidates for solid-state battery applications due to their high lithium-ion conductivity (comparable to liquid electrolytes) and favorable ductility, which allows for formation of low-resistance interfaces with active materials.[11] There are many promising classes of sulfide SSEs, including glasses, $Li_7P_3S_{11}$, LGPS materials, and the argyrodites.[12] The argyrodites, with the chemical formula Li_6PS_5X (X = Cl, Br, I), are of particular interest due to their combination of high ionic conductivity (up to 12 mS cm^{-1}), low activation energy (as low as 0.16 eV), good stability against Li

Chemical and Biological Engineering, Colorado School of Mines, Golden, CO, USA. E-mail: cwolden@mines.edu

† Electronic supplementary information (ESI) available: Additional Li_2S-m characterization, Nyquist plots, and supplementary results and discussion. See DOI: https://doi.org/10.1039/d3ta00076a

metal anodes, favorable ductility, and availability of scalable synthesis methods.[13]

However, one drawback of sulfide SSEs is the high cost of precursor materials, especially Li_2S, which has an estimated bulk price >700 USD per kg, due to the intensive/hazardous conditions required for its synthesis.[14] Nanocrystalline Li_2S is of particular interest because it has been shown to be beneficial for the mechanochemical synthesis of sulfide SSEs,[15] cathode performance,[16] and as a reagent for metal sulfide synthesis.[17] Currently, the industrially relevant Li_2S synthesis methods include the carbothermal reduction of Li_2SO_4 – a highly endothermic reaction conducted around 1000 °C that directly emits large amounts of CO_2 – and the sulfurization of Li_2CO_3 or LiOH with H_2S – reactions that off-gas a corrosive mixture of unreacted H_2S and steam in addition to CO_2.[18] Alternatives have been developed, such as the catalytic reaction of Li metal and sulfur or the reaction of Li metal and H_2S *via* a dissolved alkoxide intermediate.[15,16,19] While these approaches arguably reduce energy intensity and CO_2 emissions, the high cost and reactivity of Li metal constrain their use at commercial scale.

Recently, we and others reported a new approach to synthesizing Li_2S *via* metathesis of low-cost, abundant LiCl and Na_2S.[20–22] The reaction (eqn (1)) can be conducted at ambient temperatures in ethanol, with sparingly soluble NaCl precipitating out of solution.

$$2LiCl + Na_2S \rightarrow Li_2S + 2NaCl \quad (1)$$

The Li_2S could be recovered from the supernatant by solvent evaporation and further annealing at ≥300 °C. However, the resulting Li_2S contained oxygenated impurities – namely LiOH, Li_2CO_3, Li_2O, and Li_3OCl – that are not typically observed when Li_2S is simply dissolved and recovered from ethanol.[23–25] A preliminary study found that Li_3OCl formation could be minimized by adding 1–2% stoichiometric excess of the Na_2S reagent to drive complete consumption of the LiCl precursor. However, Li_2CO_3 and Li_2O impurities persisted. The impact of these impurities on SSE ion conduction was studied by fabricating a model Li_6PS_5Cl argyrodite and comparing to a control obtained from high-purity commercial Li_2S. It was found that the Li_2S impurities manifest as Li_3PO_4 and LiCl impurities in the argyrodite. Surprisingly, higher ionic conductivity was not necessarily correlated to lower impurity concentration, with some of the least pure electrolytes possessing higher lithium-ion conductivity than the control. Nevertheless, the role these impurity phases may play during long-term battery operation is unclear, so minimization of these side phases is desirable for large-scale deployment of the metathesis synthesis of Li_2S.

To complicate matters further, these impurities were not detected consistently in recent reports. For example, while Lisenker and Culver also reported detecting oxygenated impurities in Li_2S produced by metathesis in ethanol, Fang *et al.* did not.[21,22] This difference in purity may be attributed to differences in processing. For example, Lisenker and Culver reported sensitivity of the Li_2S purity to Na_2S stoichiometry similar to our previous reports. They also found that addition of elemental sulfur to the reaction mixture or Li_2S before annealing could improve the purity. Fang *et al.* on the other hand reported oxygen rich impurities attributed to residual solvent detected with EDAX, which they removed by annealing at 600 °C. In addition, both groups reported a reduction in NaCl concentration in the Li_2S by means of adding excess LiCl to the reaction mixture leading to precipitation of NaCl from solution *via* the common ion effect. Fang *et al.* were successful at reducing NaCl impurities this way and removed residual LiCl from the Li_2S product by washing with THF, and no oxygenated impurities were reported. However, Lisenker and Culver found little impact of LiCl excess on oxygenated impurities, and additional sulfur was instead added to prevent their formation. In a separate experiment, we showed that reacting LiCl with a sub-stoichiometric amount of Na_2S results in Li_3OCl formation along with LiCl, and that a slight excess of Na_2S is required to abate the Li_3OCl phase (Fig. S1†). Therefore, the common ion effect alone cannot account for the variation in purity reported in the literature.

In this work, we investigate the fundamental mechanism of impurity formation during the metathesis reaction in ethanol. For the first time, we demonstrated that Li_2S can in fact undergo alcoholysis with ethanol resulting in formation of lithium ethoxide. However, we found that Li_2S is kinetically stable in ethanol solutions and can be dissolved and recovered with minimal retention of solvent impurities under carefully controlled conditions. Na_2S however, is highly reactive with ethanol and undergoes alcoholysis in parallel with metathesis leading to the kinetic entrapment of EtONa in the final Li_2S. The presence of EtONa is detected with TGA, and the decomposition products are in good agreement with literature reports. This impurity formation mechanism may shed light on the apparent discrepancies reported in the recent literature concerning the metathesis synthesis of Li_2S. With this mechanism in mind, several strategies to avoid or remove oxygenated impurities were developed, with the resulting Li_2S being applied to the synthesis of Li_6PS_5Cl to elucidate underlying composition–property relationships. It was found that complete removal/decomposition of organic impurities is key to achieving both high lithium and low electron conductivity. One purification step in particular – drying of the Li_2S under a mixture of 10% H_2S in Ar at 80 °C – retained the desired nanocrystalline morphology and resulted in Li_6PS_5Cl with purity and performance essentially identical to a control material fabricated from high-purity Li_2S.

Experimental methods

Materials

Na_2S hydrate flakes (60 wt%, Sigma) were purified as reported previously.[26] Briefly, 100 g was dried by grinding followed by heating under vacuum to 70 °C overnight, then again overnight at 150 °C to yield ~60 g dehydrated Na_2S (Na_2S-d). The dehydrated material is anhydrous but retains minor polysulfide and oxy-sulfur impurities. The Na_2S-d was further purified by heating at 600 °C under flowing 50% H_2/Ar for 12 h in a packed bed configuration resulting in reduced Na_2S (Na_2S-r). Commercial Li_2S (Li_2S-c, 99.9%, Alfa) was employed as a control. LiCl (99%, Sigma) was ground and dried at 150 °C under vacuum

overnight. Ethanol (EtOH, <0.005% H_2O, Sigma), 1-propanol (PrOH, <0.005% H_2O, Sigma), tetrahydrofuran (THF, unstabilized, 99%, Alfa), P_2S_5 (99%, Sigma), sulfur (99.5%, Alfa), H_2S (10% in argon, Praxair), and Ar (99.999%, general air) were also employed. Procedures were conducted in an Ar-filled glovebox.

Sample preparation

Solvent compatibility. The compatibility of Li_2S with EtOH and/or PrOH was studied. First, sufficient Li_2S-c was added to the solvent to form a suspension above the saturation limit. Then, additional solvent was added 1 mL at a time with 1 h stirring until all Li_2S was dissolved. The solubility of Li_2S at room temperature was ~0.7 M in EtOH and ~0.4 M in PrOH. The compatibility of Na_2S with EtOH was studied by dissolving Na_2S-r in EtOH at 0.7 M for 12 h. For both Li_2S and Na_2S, a small amount of suspended solid persists in each solvent and can't be dissolved even at lower concentrations and is removed by centrifugation. This is also reported by others, and Li_2S solutions are typically settled before use.[27,28] The Li_2S/Na_2S was recovered from solution using solvent evaporation as described in the text. EtOLi was prepared for comparison by adding 0.15 g Li to 15 mL EtOH with stirring until completely dissolved, then drying under vacuum at 80 °C for 2 h.

Li_2S synthesis. LiCl was dissolved in 60 mL EtOH to obtain a 1.4 M solution. Next, Na_2S-r (2% stoichiometric excess) was added then stirred for 12 h. The resulting suspension was centrifuged at 4000 rpm for 15 minutes, then the supernatant was decanted and evaporated in an oil bath with temperature and drying time noted in the text. Metathesis Li_2S (Li_2S-m) was recovered and ground with mortar and pestle into a powder, then annealed in a 13 mm tubular fluidized bed dryer oriented vertically in a tube furnace under 100 sccm gas flowing upwards through the bed to provide fluidization. The furnace was heated at 5 °C min^{-1} to the target temperature. Additional syntheses were performed to study the impact of Na_2S purity and alcohol chain length. In the first, Na_2S-d (5% excess) was added to a 1.4 M LiCl–EtOH solution. In the latter, Na_2S-r (2% excess) was added to a 0.8 M solution of LiCl in PrOH.

Solid-state metathesis reactions were conducted by grinding LiCl with Na_2S-r (2% excess) by mortar and pestle, then heating under flowing Ar at 5 °C min^{-1} to the target temperature for 2 h. The sample was allowed to cool naturally, then ground and stirred in EtOH for 12 h at a nominal Li_2S concentration of 0.7 M. The resulting suspension was centrifuged and dried according to the above procedure.

Li_6PS_5Cl synthesis. Li_6PS_5Cl was synthesized similar to a previous report.[20] Stoichiometric quantities of Li_2S, LiCl, and P_2S_5 were ground by hand, then ball milled in a ZrO_2 jar (40 mL) with 4 ZrO_2 balls (10 mm) for 10 h in a SPEX mill (8000 M). Pellets were pressed at 320 MPa, then heated at 10 °C min^{-1} to 550 °C for 1 h in a quartz tube under dynamic vacuum.

Materials characterization

X-ray diffraction (XRD) was measured on a Philips X'Pert X-ray diffractometer with Cu Kα radiation (λ = 0.15405 nm) between 10 and 70° at a scan rate of 2° min^{-1}. Samples were prepared on a glass slide covered with Scotch Magic Tape to prevent undesired reactions with ambient moisture. Contributions from the quartz slide and tape were background subtracted with a polynomial fit. Thermogravimetric analysis (TGA) was performed with a TGA Q50 (TA Instruments) under flowing Ar by heating the furnace at a rate of 10 °C min^{-1}. Differential Scanning Calorimetry (DSC) was performed on an SDT Q600 (TA Instruments) under flowing Ar with a 10 °C min^{-1} heating rate and natural cooling. Fourier-transform infrared spectroscopy (FTIR) was performed with a Nicolet Summit FTIR spectrometer using an attenuated total reflection (ATR) accessory equipped with a diamond crystal. Field emission scanning electron microscopy (FESEM) images were taken on a JEOL JSM-7000F FESEM instrument with an accelerating voltage of 5 kV. Energy-Dispersive Analysis of X-rays (EDAX) was performed on the same instrument at 15 kV. On-line gas analysis was performed with a quadrupole mass spectrometer (Stanford Research Systems RGA200).

Electrochemical measurements

Samples were ground with mortar and pestle, then pressed into 12 mm diameter pellets in a PEEK split cell with stainless steel plungers under a uniaxial fabrication pressure of 320 MPa. Electrochemical testing was conducted with a Gamry Interface 1000E potentiostat under 120 MPa applied pressure. Electrochemical impedance spectroscopy (EIS) was performed in the frequency range of 1 Hz to 1 MHz with a 10 mV perturbation. Non-ambient temperature testing was performed by heating the split cell apparatus with an electrical heating element and allowing it to stabilize at the target temperature for 1.5 h. Bulk ionic resistance was measured from the resulting Nyquist plots one of three ways: if no high-frequency semicircle was observed, then the high-frequency *x*-axis intercept was taken as the ionic resistance. If a semicircle was detected, the impedance data was fit to the equivalent circuit shown in Fig. S5h,† and the total resistance was taken as ionic resistance. Finally, for the sample prepared from the 200 °C annealed Li_2S-m, which displayed two semicircles, ionic resistance was calculated the same, except an additional RQ element was added to the equivalent circuit in series. DC polarization was performed by applying a step voltage of 0.1 V and measuring the current response. Electronic resistance was calculated from the average of the current over the final 60 s and the applied voltage using Ohm's law.

Results and discussion

The relationship between metathesis Li_2S composition and annealing temperature was investigated using a combination of XRD and FTIR spectroscopy (Fig. 1a and b). After drying at 80 °C under vacuum, only nanocrystalline Li_2S is detected in XRD as evidenced by the broad signature peaks, but FTIR reveals the presence of residual EtOH impurities. Li_2S is IR transparent except for the large absorption peak at 400 cm^{-1} and the minor peak observed around 500 cm^{-1}. Annealing at 200 °C improves the crystallinity of the Li_2S, as indicated by the increased peak sharpness in XRD and reduced signal-to-noise ratio. However,

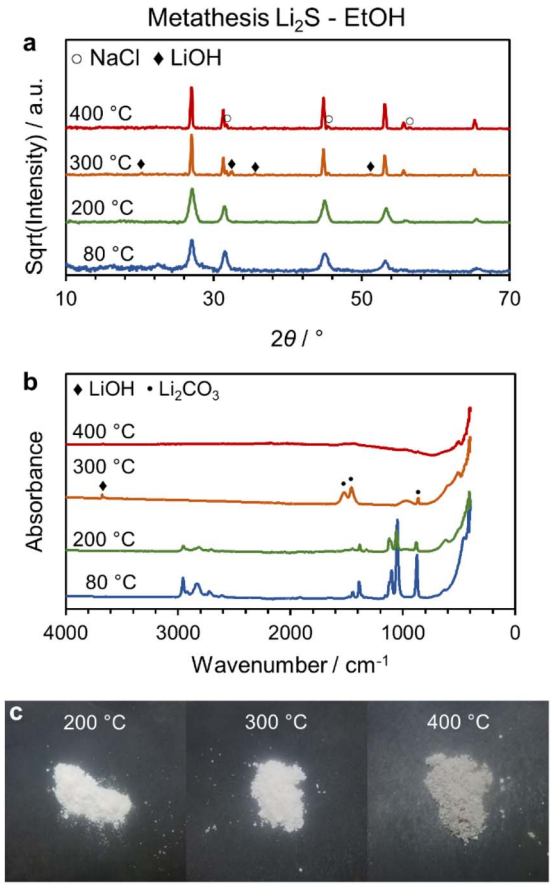

Fig. 1 (a) XRD, (b) FTIR, and (c) optical images of the Li_2S-m at different drying/annealing temperatures under Ar.

FTIR indicates that EtOH impurities are retained at 200 °C. After annealing at 300 °C, no EtOH impurities can be detected, but Li_2CO_3 and LiOH are observed. XRD and FTIR suggest that these impurities may be avoided by annealing at 400 °C, with only residual NaCl byproduct detected in XRD. This observation may be in line with the report of Fang *et al.* who used a 600 °C anneal to remove oxygenated impurities from metathesis Li_2S.[21] However, it is apparent that in this work high temperatures simply favored the formation of alternate impurities judging from the stark change in color between the 200/300 °C samples and the 400 °C sample (Fig. 1c). The grey discoloration of the 400 °C sample was linked to graphitic carbon *via* Raman spectroscopy previously,[20] and as will be shown later, the formation of carbon impurities by high-temperature annealing of solvent residues has a significant impact on the resulting SSE electronic conductivity. Higher temperature anneals also cause restructuring of the Li_2S grains as evidenced by reduced peak broadening in XRD and changes in the particle size and shape as seen in SEM (Fig. S2†). At 200 °C the Li_2S adopts a disordered flake structure, while at 400 °C it adopts a smoother, denser morphology. An intermediate form is observed after annealing at 300 °C consisting of uniform spheres of ~0.1–0.5 μm attached to the surface of the flakes.

The formation of impurities initially seemed inconsistent with literature reports. For example, Li_2S has been synthesized in EtOH by reacting H_2S and a solution of EtOLi. The Li_2S was recovered from solution by evaporating the solvent and annealing at ≥200 °C with no formation of any of the impurities shown in Fig. 1.[15] Likewise, the dissolution of Li_2S in EtOH followed by recovery through solvent evaporation is commonly employed to generate Li_2S nanoparticles for use as cathode active materials with claims of yielding pure Li_2S.[23–25] However, close review of the literature reveals several reports in which notable impurities can be detected. For example, in some reports[29,30] the presence of a diffraction peak around 32–35° (Cu Kα radiation) suggest the presence of LiOH or Li_2O. In other reports,[27,31] diffraction peaks are reported at approximately 10.5, 25.5, 29.5, and 35.0°, which matches well with the alkoxide EtOLi (Fig. S3a†). Though Li_2S has been reported to be unreactive with EtOH,[23] these other reports may suggest that is not necessarily true, with resulting purity dependent on processing, and that in some cases the Li_2S may undergo alcoholysis (eqn (2)).

$$Li_2S + EtOH \rightleftarrows LiHS + EtOLi \quad (2)$$

To investigate the effect of solvent evaporation parameters on ethoxide formation, commercially obtained high-purity (99.9%) Li_2S was dissolved in anhydrous EtOH, then evaporated under different conditions. Four combinations of high and low temperature and pressure were tested: RT/vacuum, RT/~1 atm Ar, 80 °C per vacuum, and 80 °C/~1 atm Ar. The results (XRD, FTIR, and TGA) are presented in Fig. S3† alongside the EtOLi control. XRD shows that both samples evaporated at RT (taking several days to fully dry) exhibit signatures of EtOLi. The sample dried at RT/~1 atm also exhibits unique XRD reflections that might indicate the presence of a crystalline solvate, since TGA indicates the sample retains a high concentration of loosely bound solvent. XRD of the material dried at 80 °C/~1 atm shows no evidence of EtOLi or solvate, though the broad Li_2S peaks may mask minor impurity phases (Fig. S3a†). FTIR of all samples shows similar peaks to the EtOLi, which in turn can be attributed to C_2H_5 groups by comparison with the spectra of pure EtOH (Fig. S3b†). Similar to EtONa, EtOLi exhibits a distinctive thermal decomposition, with abrupt mass loss at 217 and 393 °C. By analogy with EtONa, the first mass loss may be attributed to decomposition of a solvent complex, while the second mass loss is attributed to decomposition of the ethoxide group to solid oxygenated Li compounds (*e.g.* Li_2CO_3 and LiOH), carbon, and small gas molecules.[32] These signature mass losses can be observed in the RT/vacuum, RT/~1 atm, and 80 °C/~1 atm samples in varying degrees (Fig. S3c and d†).

Optimal purity was achieved with the 80 °C per vacuum dried sample, which shows only crystalline Li_2S by XRD with no EtOLi signature mass losses in TGA. Annealing this sample at 200 °C results in high-purity Li_2S showing no impurity signatures in XRD and only faint absorption bands in FTIR that may indicate the presence of trace amounts of solvent impurities such as EtOLi (Fig. 2a and c). These results suggest that alcoholysis can proceed but may be attenuated by rapidly removing solvent

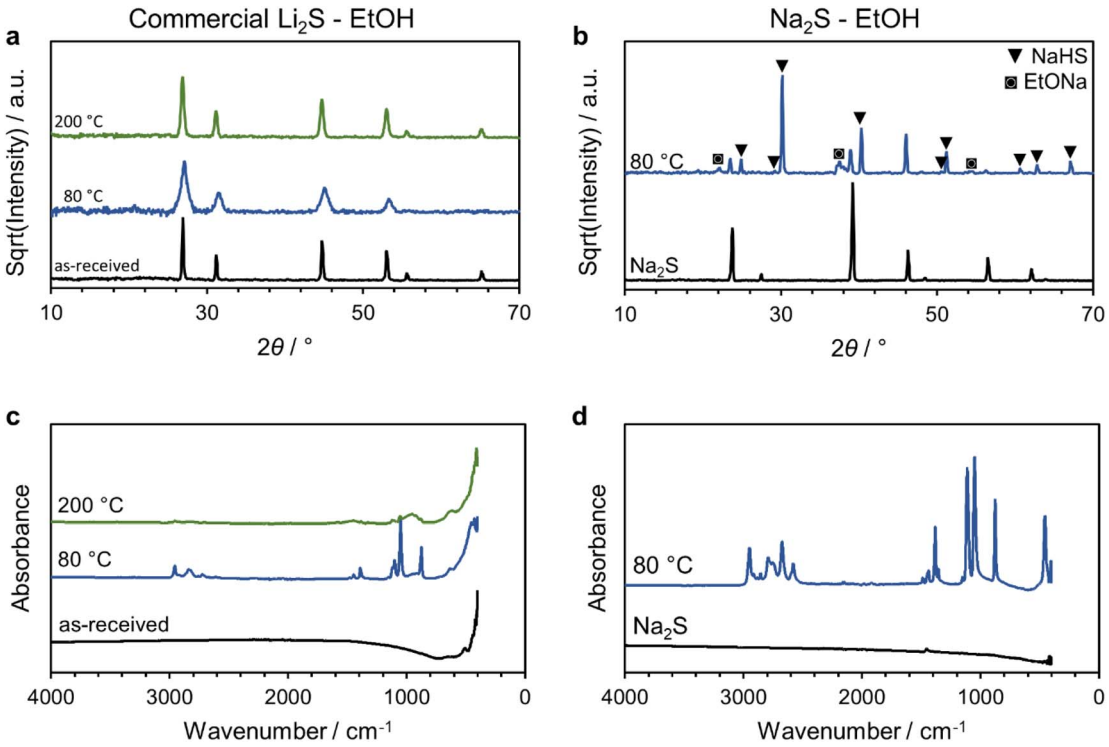

Fig. 2 (a and b) XRD and (c and d) FTIR of Li_2S-c and Na2S-r, respectively, recovered from EtOH.

under reduced pressure with sufficiently high applied heat flux, which could have important implications not only for the metathesis synthesis, but also for any application using the Li_2S–EtOH dissolution method, such as Li_2S separations and cathode nanoparticle preparations. It is also important to note that intrinsic differences in Li_2S samples may also play a role in explaining variation among literature reports. For example, according to available SDSs, Li_2S can range in appearance from pure white (as in this study) to yellow (as depicted in at least one other study[25]), suggesting that excess sulfur may be present in samples, which could impact solvent interactions.

Since Li_2S can seemingly be kinetically stabilized in EtOH, we turned our attention on Na_2S. Na_2S purified by hydrogen reduction (Na_2S-r) was dissolved in anhydrous EtOH at the same concentration as Li_2S, then dried under vacuum at 80 °C. In stark contrast to Li_2S, Na_2S is nearly completely decomposed in EtOH *via* alcoholysis (eqn (3)) as indicated by the NaHS and EtONa signature peaks detected in XRD, along with the strong IR absorption bands consistent with high concentrations of solvent impurities (Fig. 2b and d).

$$Na_2S + EtOH \rightleftarrows NaHS + EtONa \quad (3)$$

Fig. 3 shows a direct comparison of the TGA curves and their derivatives of Li_2S-m and Li_2S-c recovered from EtOH by annealing at 200 °C. The Li_2S-c sample shows negligible mass loss until 400 °C, where a slight peak in the derivative may indicate the presence of residual EtOLi. The subsequent mass loss may be attributed to LiOH volatilization and decomposition to Li_2O and H_2O,[33] and only 1.5 wt% is lost in total. The Li_2S-m sample, however, exhibits a sharp mass loss at 374 °C, which is consistent with the TGA curve of EtONa.[32] The gradual mass loss up to 300 °C may be attributed to the slow decomposition of a solvent-EtONa adduct. The subsequent mass loss above 400 °C is attributed again to LiOH, with a total mass loss of 5.4 wt% up to 600 °C.

The reactivity of Na_2S with EtOH coupled with observation of the TGA signature of EtONa suggests that the oxygenated impurities in Li_2S-m originate from kinetically entrapped

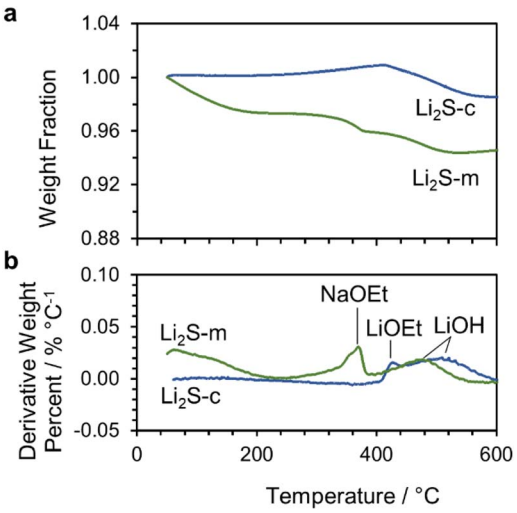

Fig. 3 (a) TGA and (b) derivative of TGA signal for Li_2S-c and Li_2S-m recovered from EtOH and annealed at 200 °C under Ar.

EtONa formed as a result of Na_2S alcoholysis, which occurs in parallel with the desired metathesis reaction (Fig. 4a). Given this mechanism of impurity formation, several strategies to remove them or prevent their formation can be proposed (Fig. 4b). The simplest approach is to physically separate the EtONa from the dried Li_2S-m using a solvent wash. THF was selected as the washing solvent since it dissolves many polar/nonpolar compounds (including the similar EtOLi), possesses a relatively low boiling point, and exhibits good compatibility with Li_2S. An alternative approach is to avoid the formation of EtONa completely by performing reaction and NaCl separation independently of each other. For example, by conducting metathesis in the solid state (SSM) at elevated temperatures in the absence of solvents, the decomposition of Na_2S could be avoided. The synthesized Li_2S can then be extracted from the reaction product with EtOH. Finally, the ethoxide byproducts could also be removed by heating the sample under a sulfur-rich environment, favoring the formation of Li_2S/Na_2S over oxygenated species. To this end, H_2S and elemental sulfur were investigated as sulfurizing agents.

Characterization of the Li_2S-m produced from each of the four purification approaches is summarized in Fig. 5 and compared to Li_2S-m annealed at 200 °C with no purification attempts as a baseline. The baseline sample shows only XRD peaks attributed to Li_2S. However, FTIR shows strong absorption bands attributed to ethoxide groups and complexed solvent molecules. The THF-washed sample was dried at 80 °C under vacuum, then ground and suspended in THF for 1 hour followed by centrifuging three times. The wet powder was dried under vacuum at RT for 1 h then annealed at 200 °C under Ar. The resulting Li_2S displays greatly reduced FTIR solvent signatures compared to baseline. This result may explain the lack of oxygenated impurities such as Li_3OCl in the report of Fang *et al.* who utilized a THF-wash to remove residual LiCl, which was added to remove NaCl from the Li_2S solution *via* the common ion effect.

The SSM approach was first investigated by performing DSC on a mixture of LiCl and 2% excess Na_2S-r (Fig. S4a†). The heat flow curve shows a strong irreversible exothermic event starting at 540 °C, and TGA shows no mass loss until 710 °C accompanied by a reversible endothermic event that may be attributed to melting/recrystallization of the reaction product. Follow-up experiments were conducted ex situ by heating mixtures of the reagents at different temperatures in a tube furnace under

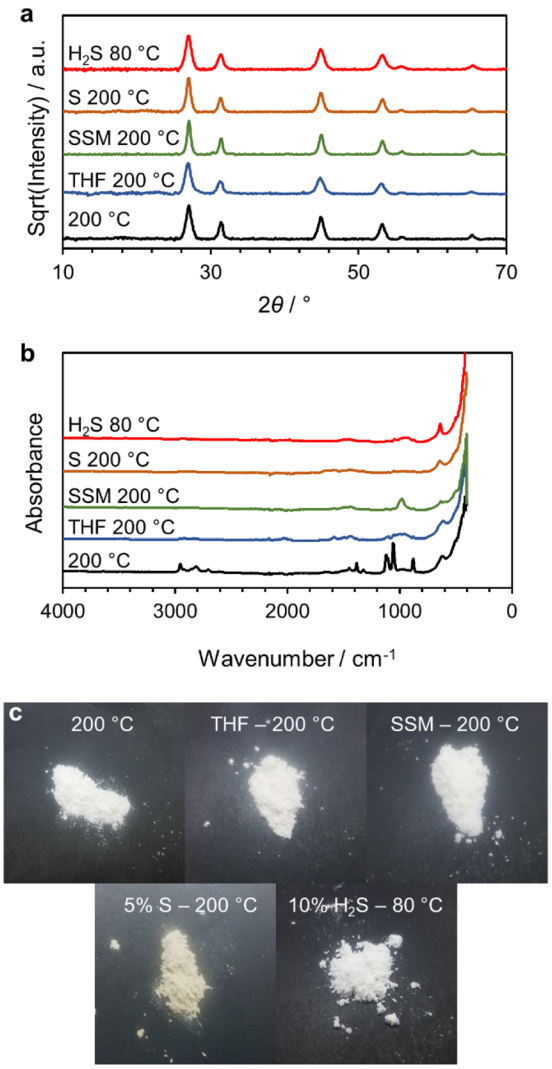

Fig. 5 (a) XRD, (b) FTIR, and (c) optical images of Li_2S-m produced using different procedures.

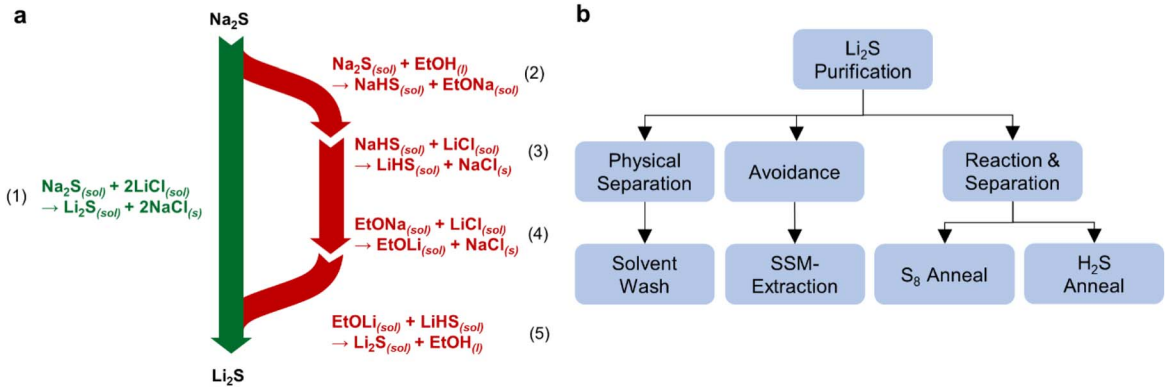

Fig. 4 (a) Reaction mechanism for formation of alkoxides. (b) Outline of approaches to preventing/removing alkoxide impurities.

flowing Ar and conducting XRD on the resulting material (Fig. S4b†). The results showed that, while the reaction can be initiated at temperatures as low as 500 °C, heating at 600 °C for 2 h is sufficient to achieve complete reaction, resulting in a solid mixture of Li_2S and NaCl with no detectable byproducts. After suspending the product powder in EtOH at a nominal Li_2S concentration of 0.7 M (identical to liquid-state metathesis), the resulting supernatant was dried at 80 °C under vacuum and annealed at 200 °C. Only Li_2S signatures are detected in XRD, and FTIR shows a significant reduction in vibrational bands from solvent impurities. However, one significant FTIR peak was detected at 955 cm^{-1}, which may be attributed to SO_3^{2-} symmetric stretch resulting from partial oxidation at elevated reaction temperatures.

Next, annealing in the presence of elemental sulfur was investigated by mixing different percentages of sulfur with the dried Li_2S. FTIR shows that intermediate sulfur loadings ~5 wt% (relative to the Li_2S mass) are preferred when annealing at 200 °C, with 1 wt% sulfur providing no benefit to solvent removal, and 10% causing the formation of additional species (Fig. S5a†). Next, annealing temperature was explored, with the expectation that excess covalent sulfur (visible as a yellow discoloration in Fig. 5c) could be removed above the sublimation point of sulfur (~100 °C). This approach was used by Lisenker and Culver who added elemental sulfur to metathesis-derived Li_2S and annealed at 400 °C, resulting in greatly reduced detection of oxygenated impurities in XRD.[22] However, in our work higher temperatures favored the formation of oxidized impurities such as Li_2CO_3 and potentially SO_3^{2-} moieties (Fig. S5b†). Additionally, some excess sulfur preferentially reacts with the sulfide to form a dark colored material that may be attributed to polysulfides (Fig. S5c†).

Finally, annealing the Li_2S under a 10% H_2S/Ar mixture was studied. The Li_2S was heated to 150 °C under flowing 10% H_2S, and the effluent was monitored with on-line mass spectrometry (Fig. S6a†). It showed a sudden consumption of H_2S starting at 77 °C, which rebounded to the baseline value after ~10 min, suggesting that H_2S drying could be a rapid, low-temperature method of removing the alkoxide byproducts. Though the use of H_2S gas raises concerns for safety, the consumption of H_2S was estimated at only ~0.05 mol H_2S per mol-Li_2S by integration of the H_2S consumption in Fig. S6a,† and concentrated H_2S was not required. Future studies will explore the possibility of using further diluted H_2S and H_2S generated on-demand (*e.g.* by using an H_2S generator[34]) or *in situ* (*e.g.* by thermal decomposition of organosulfur compounds[35]).

Separate experiments were conducted by heating the Li_2S under 10% H_2S to a target temperature for 2 h. FTIR of the resulting samples shows a monotonic reduction of impurity signatures with decreasing annealing temperatures down to 80 °C. This is significant because, while Li_2S precipitates from EtOH in nanocrystalline form, annealing at high temperatures for long times causes Ostwald ripening of the crystallites leading to increased particle sizes. The crystallite size of the H_2S dried material is estimated at 11 nm based on a Scherrer analysis of the XRD peak broadening. In a previous study we found that Li_2S nanocrystals recovered from ethanol reduced the ball milling time required to synthesize glassy sulfide SSEs.[15] While this was beyond the scope of the current study, preservation of the nanocrystallinity of the synthesized Li_2S could be beneficial to reduce the reaction time for the mechanochemical synthesis of other SSEs. In addition, small particle size is crucial to utilization of Li_2S as a cathode material, with 10 nm particle size being key to obtaining near theoretical capacity on the first charge.[16]

Optical images of all samples are shown in Fig. 5c. With the exception of the sulfur-annealed sample, all are fine white powders suggesting the absence of carbon or polysulfide byproducts. SEM images are provided in Fig. 6. All samples annealed at 200 °C possess a similar disordered flake morphology. The H_2S-dried sample has a much finer structure consisting of smaller, more dispersed crystallites. This fine-grained structure is also reflected at the macroscopic scale as seen in the optical images.

To investigate the impact of Li_2S processing and composition on electrolyte properties, Li_6PS_5Cl argyrodites were prepared from the Li_2S-m samples purified through the methods presented above by ball milling stoichiometric quantities of Li_2S, P_2S_5, and LiCl followed by annealing at 550 °C. Resulting argyrodites were compared to control samples prepared from Li_2S-c and Li_2S-m annealed at 300 °C to decompose the alkoxide intermediates to Li_2CO_3 and Li_2O as described in a previous report.[20] XRD of the argyrodite samples is presented in Fig. 7a. The material synthesized from 99.9% pure commercial Li_2S is identified as phase-pure Li_6PS_5Cl with no other impurities. When the baseline Li_2S sample annealed at 200 °C (containing intact alkoxide residue) is used to synthesize the SSE, poorly crystalline Li_6PS_5Cl results with significant Li_3PS_4 and LiCl side phases identified, possibly due to a sub-stoichiometric amount of Li_2S. Additional phases can be observed, but are difficult to identify with certainty. The Li_2S-m sample annealed at 300 °C results in much higher purity but retains traces of Li_3PO_4 and LiCl.

The THF-washed Li_2S results in promising Li_6PS_5Cl purity, with nearly undetected Li_3PO_4/LiCl signatures. The SSM-derived Li_2S, on the other hand, results in the formation of Li_3PO_4, LiCl, and NaHS side products. Annealing with 5 wt% sulfur at 200 °C

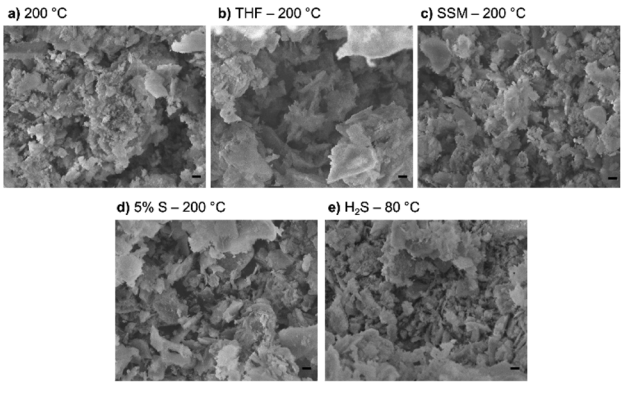

Fig. 6 SEM images of Li_2S-m produced using different procedures. Scale bar = 1 μm.

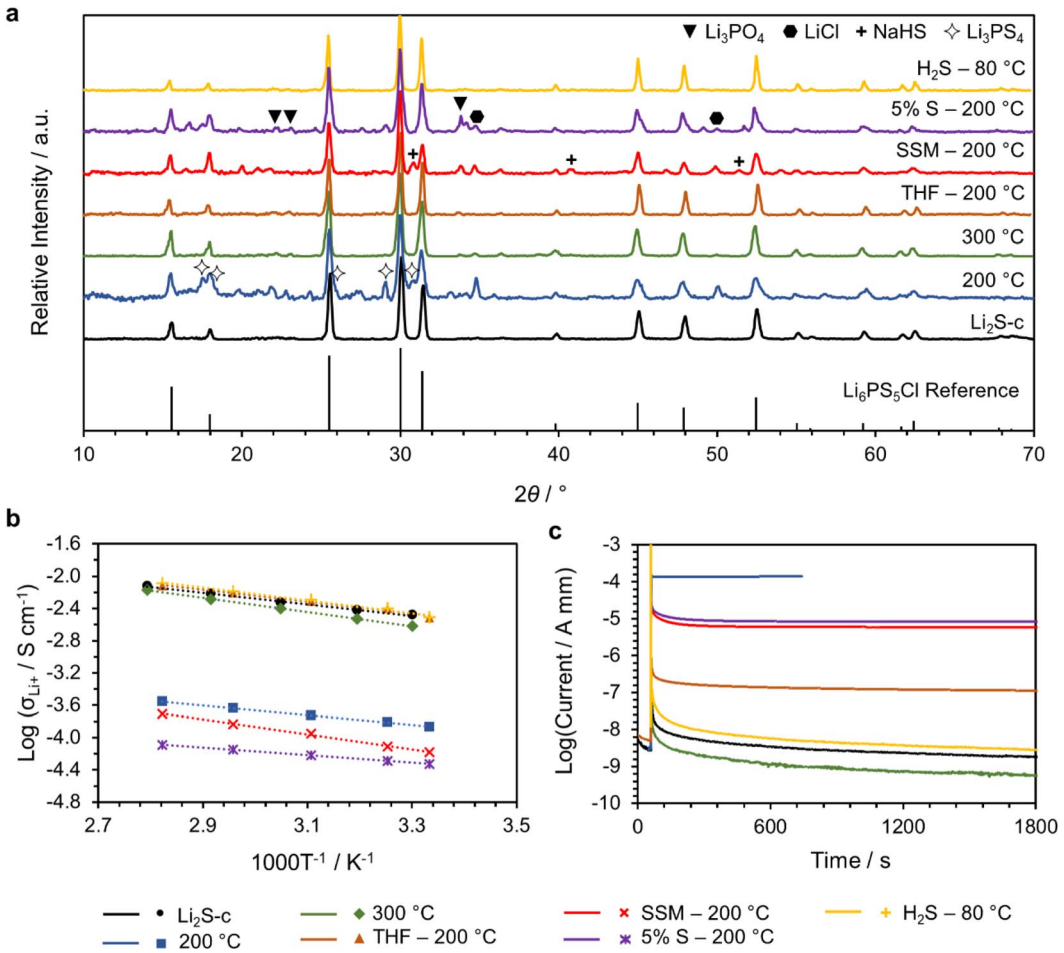

Fig. 7 (a) XRD, (b) Arrhenius plots, and (c) DC polarization current responses of Li_6PS_5Cl argyrodites fabricated from different Li_2S samples.

apparently was not sufficient to prevent impurity formation since the Li_3PO_4 and LiCl diffraction peaks are more intense than in the 300 °C annealed material. Finally, the H_2S-dried Li_2S-m material yielded the optimal purity of all metathesis samples with essentially phase-pure argyrodite forming similar to that fabricated from commercial Li_2S.

The ionic and electronic conductivity of the argyrodites was measured with EIS and DC polarization, respectively. The Arrhenius plots of ionic conductivity and DC polarization current responses are presented in Fig. 7b and c, respectively. Temperature-dependent Nyquist plots for all samples can be found in the ESI (Fig. S7†). The H_2S-dried and THF-washed Li_2S resulted in the highest conductivity of 3.1 mS cm^{-1} near ambient temperature (27–30 °C) compared to 3.3 mS cm^{-1} obtained with commercial material, which is in good agreement with leading reports in the literature.[36] The activation energies ranged from 0.18–0.19 eV. The material derived from SSM and sulfur annealing achieved below 0.1 mS cm^{-1} ionic conductivity, below that of even the baseline sample, possibly indicating the insulating nature of side phases, such as sulfur/polysulfides or NaHS.

The electronic conductivity, which is proportional to the steady-state current response in Fig. 7c, varies over 6 orders of magnitude. Low electronic conductivity is desired for solid-state separator applications to minimize leakage current, stabilize SSE-anode interfaces,[37] and prevent Li dendrite propagation.[38] The lowest electronic conductivities are achieved when Li_2S-c or Li_2S-m with H_2S drying or 300 °C annealing are used with all samples exhibiting electronic conductivity on the order of 10^{-6} mS cm^{-1}. The H_2S-dried material resulted in a low electronic conductivity, but was still ~4.5 times higher than the commercial control. The reason for this discrepancy is unknown, but could indicate further optimization of the drying temperature or procedure is needed to remove even more solvent impurities from the Li_2S-m. The highest electronic conductivity is achieved with the baseline 200 °C annealed Li_2S-m, likely due to the preferential formation of graphitic carbon when heating solvent impurities over 400 °C. The THF-washed Li_2S yielded an electronic conductivity nearly 100 times higher than the optimal samples, though much lower than other routes suggesting solvent washing is a promising approach that could be competitive with further optimization. The ionic conductivity, activation energy, and electronic conductivity are summarized for all samples in Table 1. The results show that H_2S drying at 80 °C was the optimal method for removing

Table 1 Summary of ionic/electronic properties of Li_6PS_5Cl argyrodites fabricated from different Li_2S samples

	σ_{Li} (10^{-3} S cm^{-1})	E_a (eV)	σ_e (10^{-9} S cm^{-1})
Commercial	3.3	0.18	1.4
H_2S-80 °C	3.1	0.19	6.4
300 °C	2.4	0.21	0.43
THF wash	3.1	0.18	84
SSM	0.066	0.21	4.4×10^3
5% S	0.047	0.12	6.3×10^3
200 °C	0.13	0.15	1.1×10^5

solvent impurities to maintain high SSE purity, with state-of-the-art ionic and electronic conductivities.

The goal of this work was to understand the source of impurities found in metathesis lithium sulfide and develop means to prevent or remove them. Drying under H_2S produced material of comparable purity and electrolyte performance to commercial standards, while retaining the nanocrystalline morphology that enhances its reactivity. However, other treatments may be advantageous in other applications. For example, heating Li_2S in the presence of excess sulfur can create core@shell structures of $Li_2S@Li_2S_2$, with potential advantages for improving stability in cathode applications.[39,40] Likewise, while undesirable for electrolyte applications, the electronic conductivity imparted by carbon impurities may be beneficial if the Li_2S is deployed in composite cathodes. Thus, the post processing of metathesis derived Li_2S can be used both for purification and to tailor Li_2S properties for subsequent applications.

Conclusions

Solid-state lithium batteries based on sulfide SSEs can improve the performance of energy storage devices for electromobility and load shifting applications. However, the high cost of battery-grade Li_2S constrains the large-scale synthesis of SSEs. Metathesis is a scalable method of synthesizing Li_2S from low-cost LiCl and Na_2S in ethanol, but the resulting material retains impurities. Here we demonstrate that these arise primarily through alcoholysis of the Na_2S reagent, forming impurities such as sodium ethoxide. Alcoholysis of Li_2S also occurs but at much slower rates, and its impact can be mitigated through efficient processing. Subsequent decomposition of these solvent-derived impurities during solvent removal or electrolyte synthesis leads to the formation of byproducts that negatively impact the ionic and electronic conductivity of the SSE, and may impact long-term operation when incorporated in a device. In this work, we proposed and evaluated several approaches to improving the purity of metathesis Li_2S: solvent washing, solid-state metathesis followed by solvent extraction, sulfur annealing, and H_2S drying. Among these approaches, H_2S drying at 80 °C resulted in optimal purity while retaining the nanocrystallinity (~10 nm crystallites) that has demonstrated benefits for cathode performance and electrolyte synthesis. Argyrodites synthesized from H_2S dried material exhibited purity comparable to electrolytes fabricated from high-purity commercial Li_2S with nominally identical ionic conductivity (>3 mS cm^{-1}) and electronic conductivity (~10^{-6} mS cm^{-1}).

Conflicts of interest

There are no conflicts to declare.

Acknowledgements

This work was supported by the National Science Foundation through Awards 1825470, 2219184, and the Colorado Office of Economic Development and International Trade.

References

1 J. E. Harlow, X. Ma, J. Li, E. Logan, Y. Liu, N. Zhang, L. Ma, S. L. Glazier, M. M. E. Cormier, M. Genovese, S. Buteau, A. Cameron, J. E. Stark and J. R. Dahn, *J. Electrochem. Soc.*, 2019, **166**, A3031–A3044.
2 T. M. Gür, *Energy Environ. Sci.*, 2018, **11**, 2696–2767.
3 *Battery Pack Prices Fall to an Average of $132/kWh, But Rising Commodity Prices Start to Bite*, **https://about.bnef.com/blog/battery-pack-prices-fall-to-an-average-of-132-kwh-but-rising-commodity-prices-start-to-bite/**, accessed September 23 2022.
4 J. Janek and W. G. Zeier, *Nat. Energy*, 2016, **1**, 16141.
5 C. Hendricks, N. Williard, S. Mathew and M. Pecht, *J. Power Sources*, 2015, **297**, 113–120.
6 H. Huo and J. Janek, *ACS Energy Lett.*, 2022, 4005–4016.
7 P. Bonnick and J. Muldoon, *Energy Environ. Sci.*, 2022, **15**, 1840–1860.
8 M. L. Holekevi Chandrappa, J. Qi, C. Chen, S. Banerjee and S. P. Ong, *J. Am. Chem. Soc.*, 2022, **144**, 18009–18022.
9 Y.-G. Lee, S. Fujiki, C. Jung, N. Suzuki, N. Yashiro, R. Omoda, D.-S. Ko, T. Shiratsuchi, T. Sugimoto, S. Ryu, J. H. Ku, T. Watanabe, Y. Park, Y. Aihara, D. Im and I. T. Han, *Nat. Energy*, 2020, **5**, 299.
10 K. N. Jung, H. S. Shin, M. S. Park and J. W. Lee, *ChemElectroChem*, 2019, **6**, 3842–3859.
11 S. Chen, D. Xie, G. Liu, J. P. Mwizerwa, Q. Zhang, Y. Zhao, X. Xu and X. Yao, *Energy Storage Mater.*, 2018, **14**, 58–74.
12 J. Lau, R. H. DeBlock, D. M. Butts, D. S. Ashby, C. S. Choi and B. S. Dunn, *Adv. Energy Mater.*, 2018, **8**, 1800933.
13 X. Bai, Y. Duan, W. Zhuang, R. Yang and J. Wang, *J. Mater. Chem. A*, 2020, **8**, 25663–25686.
14 H. Kwak, S. Wang, J. Park, Y. Liu, K. T. Kim, Y. Choi, Y. Mo and Y. S. Jung, *ACS Energy Lett.*, 2022, **7**, 1776–1805.
15 Y. Zhao, W. Smith and C. A. Wolden, *J. Electrochem. Soc.*, 2020, **167**, 070520.
16 Y. Zhao, Y. Yang and C. A. Wolden, *ACS Appl. Energy Mater.*, 2019, **2**, 2246–2254.
17 R. R. Chianelli and M. B. Dines, *Inorg. Chem.*, 1978, **17**, 2758–2762.
18 K. Yuan, L. Yuan, J. Chen, J. Xiang, Y. Liao, Z. Li and Y. Huang, *Small Struct.*, 2021, **2**, 2000059.

19 M. Duchardt, M. Diels, B. Roling and S. Dehnen, *ACS Appl. Energy Mater.*, 2020, **3**, 6937–6945.
20 W. H. Smith, S. A. Vaselabadi and C. A. Wolden, *ACS Appl. Energy Mater.*, 2022, **5**, 4029–4035.
21 L. Fang, Q. Zhang, A. Han, Z. Zhao, X. Hu, F. Wan, H. Yang, D. Song, X. Zhang and Y. Yang, *Chem. Commun.*, 2022, **58**, 5498–5501.
22 I. Lisenker and S. Culver, Method of Preparing a Water-Reactive Sulfide Material, *USA Pat.*, US2021/0253424A1, 2021.
23 F. Wu, A. Magasinski and G. Yushin, *J. Mater. Chem. A*, 2014, **2**, 6064–6070.
24 F. Wu, J. T. Lee, A. Magasinski, H. Kim and G. Yushin, *Part. Part. Syst. Charact.*, 2014, **31**, 639–644.
25 F. Wu, T. P. Pollard, E. Zhao, Y. Xiao, M. Olguin, O. Borodin and G. Yushin, *Energy Environ. Sci.*, 2018, **11**, 807–817.
26 W. H. Smith, J. Birnbaum and C. A. Wolden, *J. Sulfur Chem.*, 2021, 1–17.
27 C. Wang, X. Wang, Y. Yang, A. Kushima, J. Chen, Y. Huang and J. Li, *Nano Lett.*, 2015, **15**, 1796–1802.
28 Y. Zhan, H. Yu, L. Ben, Y. Chen and X. Huang, *Electrochim. Acta*, 2017, **255**, 212–219.
29 F. Han, J. Yue, X. Fan, T. Gao, C. Luo, Z. Ma, L. Suo and C. Wang, *Nano Lett.*, 2016, **16**, 4521–4527.
30 J. W. Park, J. Kang, J. Y. Koh, A. Caron, S. Kim and Y. Jung, *J. Electrochem. Sci. Technol.*, 2020, **11**, 33–40.
31 Y. Zhang, M.-X. Xie, W. Zhang, J.-L. Yan and G.-Q. Shao, *Mater. Lett.*, 2020, **266**, 127508.
32 K. Chandran, M. Kamruddin, P. K. Ajikumar, A. Gopalan and V. Ganesan, *J. Nucl. Mater.*, 2006, **358**, 111–128.
33 H. Kim, H. D. Jang and M. Choi, *Chem. Eng. J.*, 2015, **280**, 132–137.
34 B. Pocock, L. Scholten and P. Erickson, *Ind. Eng. Chem., Anal. Ed.*, 1942, **14**, 575.
35 A. Alphonse, *Thioacetamide as a Sulfur Precursor for Chalcopyrite Thin Film Solar Cells*, University of Texas at Arlington, 2009.
36 J. Wu, L. Shen, Z. Zhang, G. Liu, Z. Wang, D. Zhou, H. Wan, X. Xu and X. Yao, *Electrochem. Energy Rev.*, 2020, **4**, 101–135.
37 Y. Zhu, X. He and Y. Mo, *ACS Appl. Mater. Interfaces*, 2015, **7**, 23685–23693.
38 F. Han, A. S. Westover, J. Yue, X. Fan, F. Wang, M. Chi, D. N. Leonard, N. J. Dudney, H. Wang and C. Wang, *Nat. Energy*, 2019, **4**, 187–196.
39 X. Zhang, H. Yang, Y. Sun and Y. Yang, *ACS Appl. Mater. Interfaces*, 2022, **14**, 41003–41012.
40 S. Yang, F. Wan, A. Han, L. Fang, Q. Sun, Z. Zhao, D. Song, L. Zhang, L. Chen, C. A. Wolden, X. Zhang and Y. Yang, *J. Cleaner Prod.*, 2023, **382**, 135221.

